Journal of Integrative Agriculture 2026, 25(9): 3800–3813

Available online at ScienceDirect

Journal of Integrative Agriculture

RESEARCH ARTICLE

scRNA-seq reveals the molecular atlas of the goat follicular microenvironment over the time course of ovulation

Conghui Guo[1, 2*], Guangbin Liu[1, 2*], Jie Liu[1, 2], Kaihao Chen[1, 2], Ming Deng[1, 2], Baoli Sun[1, 2], Yongqing Guo[1, 2], Dewu Liu[1, 2#], Yaokun Li[1, 2#]

[1] *College of Animal Science/National Local Joint Engineering Research Center of Livestock and Poultry, South China Agricultural University, Guangzhou 510642, China*

[2] *Lingnan Guangdong Laboratory of Modern Agriculture, Guangzhou 510642, China*

Highlights

- Single-cell sequencing revealed cellular dynamics during goat ovulation.
- Immune-cell infiltration occurs within 6 h after the luteinizing hormone (LH)/human chorionic gonadotropin (hCG) surge.
- Granulosa cell–immune cell communication is pivotal for ovulation progression.

Abstract

Ovulation is paramount for female animal fertility, necessitating a thorough understanding of its process and molecular underpinnings. This study aimed to delineate the temporal dynamics of ovulation in the goat ovary. Utilizing single-cell sequencing, we analyzed follicular fluid samples obtained at 0, 6, 12, 18, and 24 h post-hCG administration, identifying 4 cell types and 6 myeloid cell subtypes. We elucidated gene expression and functional changes in granulosa cells (GCs) over the time course of ovulation. Notably, our study detected and confirmed immune cell infiltration at 6 h post-luteinizing hormone (LH) peak. Additionally, cell–cell communication analysis revealed strong predicted interactions between GCs and macrophages, involving signaling programs associated with immune-cell recruitment, extracellular-matrix remodeling, and oocyte maturation. Collectively, our investigation has established a comprehensive single-cell transcriptome atlas of the ovulatory goat follicular microenvironment for advancing exploration into ovulation mechanisms and developing therapies for ovulatory disorders.

Keywords: hCG, ovulation, granulosa cell, macrophages

1. Introduction

Ovulation represents a pivotal reproductive event. In livestock, ovulation rate significantly influences litter size and fecundity, thereby influencing the economic viability of farming operations. In humans, ovulatory dysfunctions are directly linked to infertility, with approximately 25% of infertility cases attributed to such disorders (Carson and Kallen 2021). Consequently, there is an imperative to deepen our comprehension of ovulation. In mammals, following sexual maturation, the body secretes gonadotropins that promote follicular development from the antral stage to maturation. This process entails a progressive accumulation of follicular fluid (FF) and enlargement of the follicular cavity. Subsequently, a surge in luteinizing hormone (LH) initiates ovulation (Direito *et al*. 2013). Human chorionic gonadotropin (hCG) can functionally replace LH in inducing ovulation in animal models (Rahman and Rao 2009). Upon LH or hCG stimulation, granulosa cells (GCs) and thecal cells within the follicle are the first to respond and exhibit heightened expression of LHCGR, activating intertwined signaling cascades that modulate cellular activities. Remarkable alterations occur in cellular composition, cell function, hormone secretion, and follicular morphology (Owen and Jaffe 2023; Zaniker *et al*. 2023). Notably, prior to ovulation, the follicular membrane undergoes vascularization, leading to basal lamina disruption and infiltration of immune cells into

Received 26 April 2024; Received in revised form 12 July 2024; Accepted 3 September 2024; Available online 26 September 2024
[#]Correspondence Yaokun Li, E-mail: ykli@scau.edu.cn; Dewu Liu, E-mail: dwliu@scau.edu.cn
[*] These authors contributed equally to this study.

doi: 10.1016/j.jia.2024.09.029

the follicular lumen (Duffy *et al*. 2019; Choi *et al*. 2023). GCs' behavior shifts during follicular development, with preovulatory GCs undergoing luteinization and participating in immune cell interactions (Turathum *et al*. 2021). Nonetheless, the intricate and dynamic nature of ovulation poses challenges to elucidating its underlying mechanisms. The cell classification, functional alterations, and intercellular interactions within ovulatory follicles remain largely unexplored.

The Chuanzhong black goat is a representative indigenous meat-goat breed in China and an important component of national livestock genetic resources. Owing to its large body size, rapid growth, high reproductive capacity, and favorable meat-production traits, this breed has considerable value for regional goat production, germplasm conservation, and genetic improvement (Huang *et al*. 2016). Nevertheless, reproductive performance is a key limiting factor for efficient goat production and may be affected by environmental adaptation after cross-regional introduction. Because ovulation directly determines oocyte release and litter size, a deeper understanding of the regulatory mechanisms governing follicular development and ovulation in Chuanzhong black goats is essential for improving reproductive efficiency and promoting the sustainable utilization of this local breed. In addition, goats more closely resemble humans than mice and pigs in terms of ovulation duration and ovulation rate (Wang *et al*. 2018; Gao *et al*. 2023; Mantri *et al*. 2024), making them a valuable large-animal model for studying mammalian ovulatory biology. Therefore, we performed 10× Genomics scRNA-seq on FF collected from Chuanzhong black goats at 0, 6, 12, 18, and 24 h after hCG administration to construct a temporal single-cell atlas of the ovulatory follicular microenvironment and to characterize dynamic cellular states and intercellular communication during ovulation.

2. Materials and methods

2.1. Animals

All animals were obtained from Leizhou Zhuangyuan Black Goat Co., Ltd., China, and all experimental protocols were approved by the Ethics Committee of South China Agricultural University. The goats were fasted overnight before euthanasia.

2.2. Sample collection and preparation

More than 30 multiparous Chuanzhong black goats approximately 3 years of age, with similar genetic backgrounds, similar weights, the same rearing environment, healthy condition, and no history of abortion, were used for the experiment. We observed 2 consecutive estrous cycles of the ewes and selected 20 goats that were in a normal estrous state for subsequent experiments. Then, intravaginal progesterone sponges (Zoetis, New Zealand) and prostaglandin (NSHF, China) treatments were used to synchronize the timing of estrus, and hCG (NSHF, China) treatment was used to synchronize the timing of ovulation. FF was collected from goat ovaries at 0, 6, 12, 18, and 24 h after hCG injection. Two goats were sampled at each time point, and the samples were mixed to yield a total of 5 samples. The mixed FF was gently pipetted to separate some of the aggregated cells. Subsequently, cells were centrifuged at 800 r min^{-1} for 5 min, and the supernatant was discarded to remove impurities. The pellet was then resuspended in 1 mL of preheated complete culture medium and centrifuged at 300 r min^{-1} for 5 min to eliminate small cells. The resulting supernatant was carefully aspirated, and the pellet was resuspended in 50 μL of pre-warmed medium. After that, cell viability was determined by trypan blue staining with a TC20 automated cell counter (Bio-Rad, Hercules, CA, USA), and the percentage of viable cells in the single-cell suspension was more than 70%. The concentration of the single-cell suspension was adjusted to 700–1,200 cells μL^{-1}.

2.3. scRNA library construction and sequencing

An appropriate number of cells was loaded into each channel of the Chromium Single Cell A Chip (v2 chemistry, PN-120236). 10× libraries were constructed using the Chromium Controller and Chromium Single Cell 3′ Reagent Kits (v2 chemistry, CG00052). In brief, single-cell suspensions in each channel of the chip were loaded on a Chromium Controller (10× Genomics, Pleasanton, CA) to generate single-cell GEMs (gel beads in emulsion). Then, 10× libraries of each channel were prepared using the Chromium Single Cell 3′ Gel Bead and Library Kit v2 (PN-120236, 120237, 120262; 10× Genomics) (Dura *et al.* 2019). Libraries were sequenced on the Illumina NovaSeq sequencer with 150-bp paired-end reads at Novogene Bioinformatics Technology Co., Ltd. (Tianjin, China).

2.4. scRNA-seq data processing

We employed fastp for initial quality assessment of raw reads. The gene-cell matrices generated by Cell Ranger served as input data for further analyses with Seurat (Hao *et al.* 2021). To ensure high data quality, we filtered out dead and low-quality cells by retaining genes expressed in more than three single cells, with each cell expressing at least 200 genes. Then, we identified the highly variable genes for clustering analysis. For principal component analysis (PCA), the scaled data were reduced to the first 50 principal components (PCs) using highly variable genes. The selection of PCs used for nonlinear dimensional reduction (t-distributed stochastic neighbor embedding, t-SNE) analysis was determined according to the elbow plot function. Visual exploration of single-cell data structures and trajectories was conducted separately using t-SNE and Uniform Manifold Approximation and Projection (UMAP).

2.5. Cell type identification

Through an extensive literature review and based on marker genes for each cell type and genes enriched in clusters, we identified the cell types for each cluster. For accurate identification, we manually and repeatedly checked the expression of marker genes in the Loupe Cell Browser.

2.6. Pathway/enrichment analysis

The cluster-enriched genes or differentially expressed genes (DEGs) with statistical significance were applied to clusterProfiler for pathway enrichment analysis. Gene

Ontology (GO) terms and Kyoto Encyclopedia of Genes and Genomes (KEGG) pathways were evaluated for significant enrichment based on the *Q*-value and *P*-value.

2.7. RNA velocity analysis and pseudotime analysis

RNA velocity analysis was used to predict the future state and differentiation trajectory of cells by assessing changes in cell status. First, Velocyto was used to generate a loom format file containing information on genome alignment and spliced and unspliced mRNA data. The loom format file subsequently served as the input for scVelo (https://scvelo.org). Finally, the results were projected onto a UMAP plot generated for visualization consistency in Seurat.

Pseudotime analysis allows inference of the evolutionary and differentiation relationships among cells, unveiling determinants of cell fate. The Monocle2 software package was utilized for this analysis (Trapnell *et al.* 2014). First, the newCellDataSet function was used to convert the expression matrix, cell annotations, and gene annotations into a Cell Data Set object. Subsequently, the setOrderingFilter function was used to select genes. Finally, trajectories were inferred, and cells were ordered according to the inferred temporal sequence.

2.8. Cell–cell interaction analysis

The goat genes were matched to their human orthologs, and based on receptor–ligand interaction information in the CellPhoneDB (https://www.cellphonedb.org) database, interaction pairs associated with the expression of two cell types were screened. A null distribution was established through random permutation of cell type labels, followed by computation of *P*-values. Significantly enriched interaction pairs were selected based on statistical significance, and the communication network between cell types was visualized.

2.9. Immunohistochemistry staining

The ovaries were fixed in 4% paraformaldehyde, dehydrated, paraffin-embedded, sectioned, and subjected to antigen retrieval. Immunostaining was performed using an anti-FSHR antibody (BC118548; Wuhan Sanying, China) and a TNFAIP6 antibody (AF5492; Affinity Biosciences, OH, USA). Images were acquired using a Pannoramic 250FLASH scanner (3DHISTECH, Budapest, Hungary) and viewed with CaseViewer 2.5.0.

2.10. Fluorescence-activated cell sorting

We collected ovarian FF at 0 and 6 h after hCG injection, after which the cells were incubated in staining buffer containing Fixable Viability Stain 700 (FVS700, BD) at room temperature for 20 min to exclude dead cells. Subsequently, the cells were washed and centrifuged at 500× g for 5 min to remove the supernatant, and the cell pellet was then blocked on ice for 20 min in staining buffer containing CD16/CD32 antibodies (clone 2.4G2). Cell surface staining was carried out by incubating cells with antibodies against CD3e (clone 145-2C11), CD11b (clone M1/70), and CD86 (clone GL1) for 50 min at 4°C after blocking with Fc antibody. All the antibodies used were purchased from BioLegend or BD Biosciences. The obtained data were analyzed using FlowJo v10.8.1 software, and the flow cytometer utilized for these experiments was the BD *LSRFortessa*™ X-20 cell analyzer.

3. Results

3.1. Single-cell transcriptomic atlas in ovulation

To investigate the cellular heterogeneity and expression profiles associated with follicle maturation and ovulation in goats, FF was collected at 0, 6, 12, 18, and 24 h after hCG treatment for scRNA-seq (Fig. 1-A). By filtering out low-quality cells with high mitochondrial/ribosomal gene content, erythrocytes, and doublets (Appendix A-a), a total of 24,553 cells were detected. For each sample (0, 6, 12, 18, and 24 h), 4,892, 4,591, 4,284, 4,166, and 6,620 cells, respectively, were captured. An average of 80,243 reads were detected for each cell (Appendix B). Utilizing a Seurat-based workflow on the sequencing data, we performed cell dimensionality reduction and clustering. UMAP analysis identified a total of 23 cell clusters (Fig. 1-B). Notably, the distribution of samples within the clusters was uneven, demonstrating clear temporal characteristics. For instance, in clusters 17 and 22, samples taken at the 24 h mark constituted over 80% of the total, indicating that these cell populations may play a role in the late periovulatory stage. Conversely, in cluster 7, approximately 70% of the samples were from the 0 h time point, suggesting that this cell population is highly represented during the initial stage of ovulation (Fig. 1-C). To better understand the features of each cluster, we displayed the top 10 variable features for each cluster in a heatmap, representing their expression specificity (Appendix A-b). This approach facilitated further analysis of the biological significance and differences among the cell clusters.

Due to the absence of a specialized gene database for goats, automatic annotation of the data was not possible. Therefore, we manually identified the cell types based on the highly expressed genes in each cluster and references to existing cell markers. In the goat FF, a total of 4 main cell populations were identified: GCs (12,164, 49.54%), T cells (3,374, 13.74%), B cells (71, 0.29%), and myeloid cells (8,944, 36.43%). We constructed a t-SNE plot based on the expression profiles of genes with defined cell type specificity (Fig. 1-E). Briefly, cells exhibiting elevated expression of *FSHR*, *CDH2*, *NMB*, *FST*, *INHA* and *MFGE8* were classified as GCs (Fan *et al.* 2021; Ge *et al.* 2023). *CD4, CTSW, GATA3*, and *CD3G* were marker genes for T cells. Cells were annotated as B cells based on the high expression of the typical cell markers *JCHAIN* and *CD79A*. Myeloid cell classification was determined by pronounced expression levels of *C1QB, AIF1*, and *PECAM1* (Mrdjen *et al*. 2018; Danaher *et al*. 2023). Average expression levels and percentages of cells expressing these marker genes were visualized in a dot plot (Fig. 1-F). Notably, a series of cell type-specific candidate marker genes were identified in goat follicular cells. These genes included *NCKAP1, IGSF11*, and *VCL* in GCs; *CD52* and *ICOS* in T cells; *MZB1* and *DERL3* in B cells; and *TIAM1, HNMT*, and *CALCRL* in myeloid cells (Fig. 1-D).

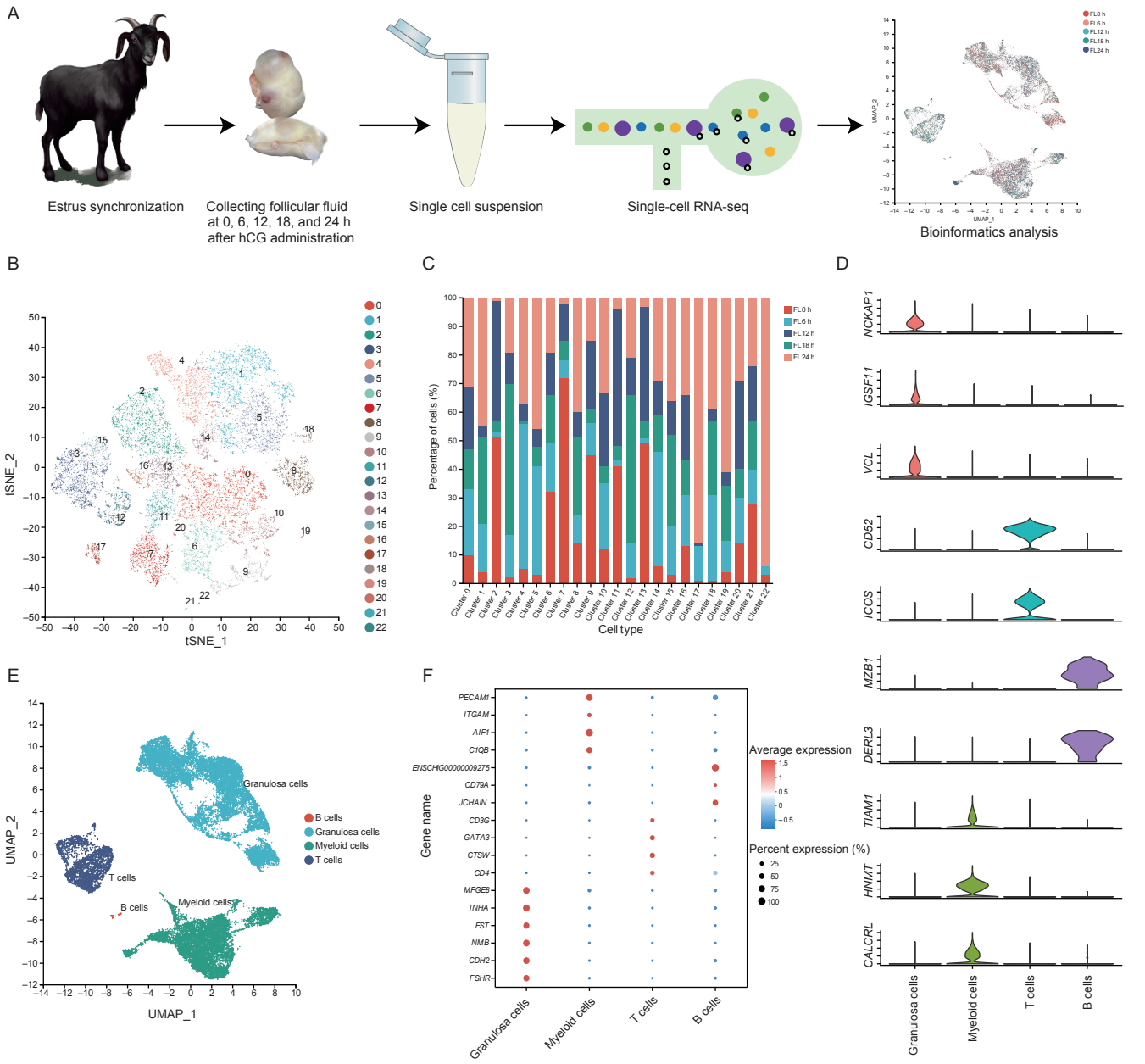

Fig. 1 Single-cell RNA-seq transcriptomics of goat follicular fluid (FF). A, flowchart of the goat FF scRNA-seq procedure. hCG, human chorionic gonadotropin. B, a total of 23 transcriptional cell clusters were revealed by unsupervised clustering and were projected on a t-SNE plot. C, proportion of sample distribution in each cluster. D, violin plots of the expression signatures of new marker genes. E, 4 ovarian cell types were visualized using Uniform Manifold Approximation and Projection (UMAP) plots. F, dot plots showing the differential expression patterns of the selected genes in each cell type.

3.2. Cellular heterogeneity within ovulatory follicles

After identifying the main cell types, we found that GCs and myeloid cells constituted the major components of the goat ovulatory follicle microenvironment, suggesting that they may play crucial roles in ovulation. To further explore cellular heterogeneity, we subdivided GCs and myeloid cells into distinct subgroups. GCs were subdivided into 8 subclusters (Fig. 2-A). Correlations and PCA among subclusters are shown in Appendix C-a and c. Subsequently, we classified the 8 subclusters into 3 cell subtypes: growing granulosa cells (g_GCs), ovulating granulosa cells (o_GCs), and atretic granulosa cells (a_GCs) (Fig. 2-A). Among them, g_GCs highly expressed *AMH, FSHR*, and *PLPPR1* (Liu *et al*. 1998) (Fig. 2-B). KEGG terms specific to g_GCs included “Signaling pathways regulating pluripotency of stem cells”, “TGF-β signaling pathway”, and “Wnt signaling pathway”, all of which regulate follicular growth, consistent with our definition of g_GCs (Fig. 2-F). o_GCs were characterized by high expression of *TNFAIP6*, *OXT*, *MCL1* and *PGRMC1* (Sayasith *et al*. 2008). Immunohistochemistry results also confirmed that FSHR was enriched in g_GCs (highly expressed in mid-sized follicles), while TNFAIP6 serves as a marker for o_GCs (highly expressed in large follicles) (Fig. 2-E). The genes specifically expressed in o_GCs mainly participate

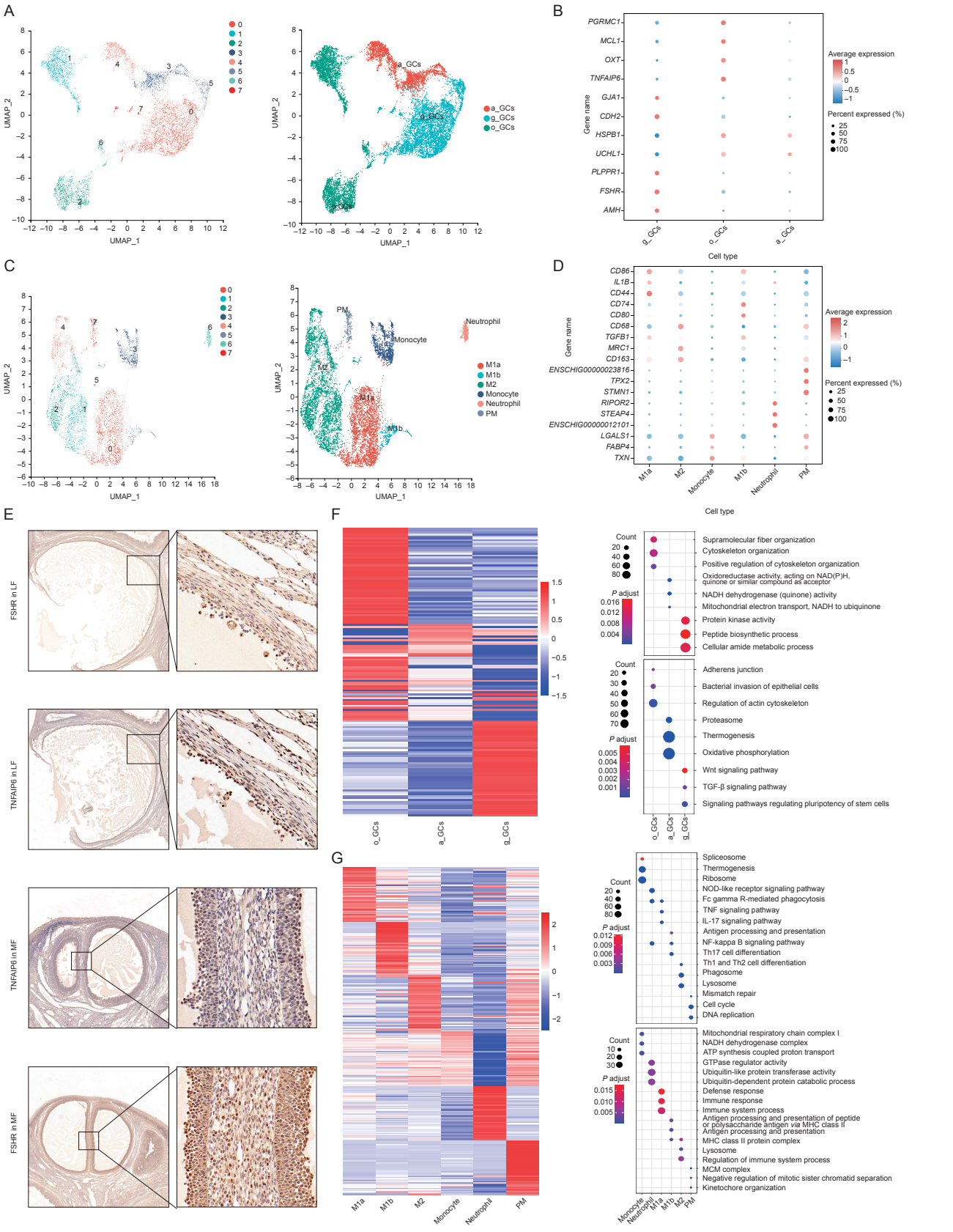

Fig. 2 Characterization of granulosa cells (GCs) and myeloid cells in ovulating follicles. A, Uniform Manifold Approximation and Projection (UMAP) plots of GC subtypes. B, dot plots showing the differential expression patterns of the selected genes associated with the GC subtypes. C, UMAP plots of myeloid cell subtypes. D, dot plots showing the differential expression patterns of the selected marker genes for myeloid cell subtypes. E, immunohistochemistry (IHC) staining of the ovary (left 2×; right 30×). LF, large follicle; MF, mid-sized follicle. F, heatmap and GO/KEGG enrichment of the top 50 genes in each cell subtype of GC. G, heatmap and GO/KEGG enrichment of the top 50 genes in each cell subtype of myeloid cells.

in cytoskeletal regulation and adhesion junction-related pathways, which are key cell biological features during follicle development and ovulation. a_GCs expressed *UCHL1* and *HSPB1*, with low or undetectable expression of *CDH2* and *GJA1* (Ge *et al*. 2023). The GO terms for a_GCs were mainly enriched in energy metabolism, which may imply that follicular atresia is an energy-consuming process.

Myeloid cells were also subdivided into 8 subclusters. Correlations and PCA between subclusters are shown in Appendix C-b and d. The myeloid cells were further categorized into 6 cell types: M1a-like macrophages (M1a), M2-like macrophages (M2), and M1b-like macrophages (M1b), proliferative macrophages (PM), monocytes, and neutrophils (Fig. 2-C). Specifically, M1b highly expressed *CD80, CD74*, and *CD86*. The terms specific to M1b included "antigen processing and presentation", "NF-κB signaling pathway", and "Th17 cell differentiation". M2 showed elevated expression of *CD163*, MRC1 (*CD206*) (Appendix D), and *CD68*. KEGG enrichment analysis revealed that M2 in FF primarily engages in processes associated with "lysosome", "phagosome", and "Th1 and Th2 cell differentiation", suggesting its phagocytic capacity and role in T-cell regulation. Cells expressing *IL1B, CD44*, and *CD86*, which promote inflammatory responses but exhibit differential gene expression compared to M1b, were classified as the M1a subtype (Solier *et al*. 2023). M1a macrophages showed GO enrichment associated with immune response and defense reactions. High expression levels of cell cycle-related genes such as *STMN1, TPX2*, and *ENSCHIG00000023816* (*MKI67*) characterize PMs (He *et al.* 2021). PMs primarily engage in functions related to "DNA replication", "cell cycle", and "mismatch repair", suggesting macrophage proliferation within ovulatory follicles. Cells expressing *TXN*, *FABP4*, and *LGALS1* were identified as monocytes (Ingram *et al*. 2019; Ruvolo *et al*. 2020), and those expressing *ENSCHIG00000012101* (*CXCR1*), *STEAP4*, and *RIPOR2* were characterized as neutrophils (Liang *et al*. 2017) (Fig. 2-D). The enrichment of monocytes in energy synthesis-related pathways implies a potential metabolic shift occurring in these cells. For neutrophils, enrichment was primarily in the FcγR, NOD-like receptor, and NF-κB signaling pathways (Fig. 2-G). In brief, our analysis of cell subtypes reveals significant cellular and molecular diversity within the FF.

3.3. Immune cells infiltrate the follicle within 6 h following the LH/hCG peak

In the ovary, immune cell populations dynamically fluctuate throughout the estrous cycle. Herein, we assessed cellular composition and observed a notable 6-fold increase in myeloid cell proportion, rising from 9.1% to 57.74% within the initial 6 h after hCG administration (Fig. 3-A). Further comparison revealed that the predominant myeloid cell subtype that increased at 6 h was M1a (Fig. 3-C). Subsequently, we conducted GO enrichment analysis on differential genes by comparing the samples at 0 and 6 h, revealing their association with energy-related pathways such as "NADH dehydrogenase (quinone) activity", "oxidoreductase activity acting on NAD(P)H", "respiratory chain complex" and "inner mitochondrial membrane protein complex". Additionally, transport-related pathways were identified, including "electron transfer activity", "proton transmembrane transporter activity", "inorganic cation transmembrane transport" and "monovalent inorganic cation transport" (Fig. 3-B). This observation underscores pronounced cellular transmembrane transport activity following hCG administration, suggesting that this process may involve cell migration. To validate the increase in immune-cell infiltration, we collected goat FF at 0 and 6 h after hCG administration and performed fluorescence-activated cell sorting. Following the removal of cellular debris and erythrocytes, we initially labeled viable cells with CD11b (ITGAM) antibodies to identify myeloid cells. Subsequently, CD86 expression was used to assess M1-like activation among myeloid cells (Fig. 3-D). The cellular expression patterns are depicted in Fig. 3-E, confirming a significant increase in M1-like myeloid activation in the goat FF 6 h post-hCG administration (P<0.05) (Fig. 3-F).

3.4. Gene expression features of GCs during ovulation

GCs constitute the primary components of the follicular microenvironment, exhibiting diverse functionalities throughout various stages of follicular maturation. During ovulation, GCs orchestrate hormone secretion, angiogenesis, and oocyte meiotic division (Grondahl *et al.* 2012). Herein, we employed a heatmap visualization to delineate the gene expression profiles specifically elevated in GCs at 0, 6, 12, 18, and 24 h post-hCG administration (Fig. 4-A).

At 0 h, GCs exhibited high expression of *FBP2*, *INHA*, *DLC1*, *MX1*, *ISG15*, *GRID2* among others. Functional enrichment was primarily focused on processes such as "mitochondrial electron transport, NADH to ubiquinone", "respiratory electron transport chain", and "NADH dehydrogenase activity", indicating that GCs generate energy through oxidative phosphorylation during this stage. At 6 h, GCs expressed *ENSCHIG00000012599*, mitochondrial calcium uniporter (*MCU*), *PDE7B*, *MARK1*, *PCLO*, etc. GO analysis at 6 h also revealed enrichment of "regulation of cell migration" and "transmembrane receptor protein tyrosine kinase signaling pathway", potentially associated with immune-cell infiltration at 6 h, as observed in Section 3.3, suggesting that GCs may contribute to immune-cell recruitment. At 12 h, GCs highly expressed *CRISPLD2*, *ADAMTS9*, *ADAMTSL1*, *RUNX2*, *CADM2*, *PGRMC1*, etc. Enriched pathways included "regulation of calcium ion transmembrane transport *via* high voltage-gated calcium channel" and "actin cytoskeleton organization". At 18 h, GCs highly expressed *IFI6*, *ENSCHIG00000009267*, *ENSCHIG00000005203*, *ENSCHIG00000020169*, *RPS26*, *ENSCHIG00000016060*, etc. GO analysis at 18 h revealed enrichment of "regulation of vascular-associated smooth muscle cell proliferation", "regulation of vascular associated smooth muscle cell migration", and "inflammatory response", suggesting the activation of inflammatory and vascular-remodeling programs that mediate immune responses during ovulation at this stage. At 24 h, GCs demonstrated elevated

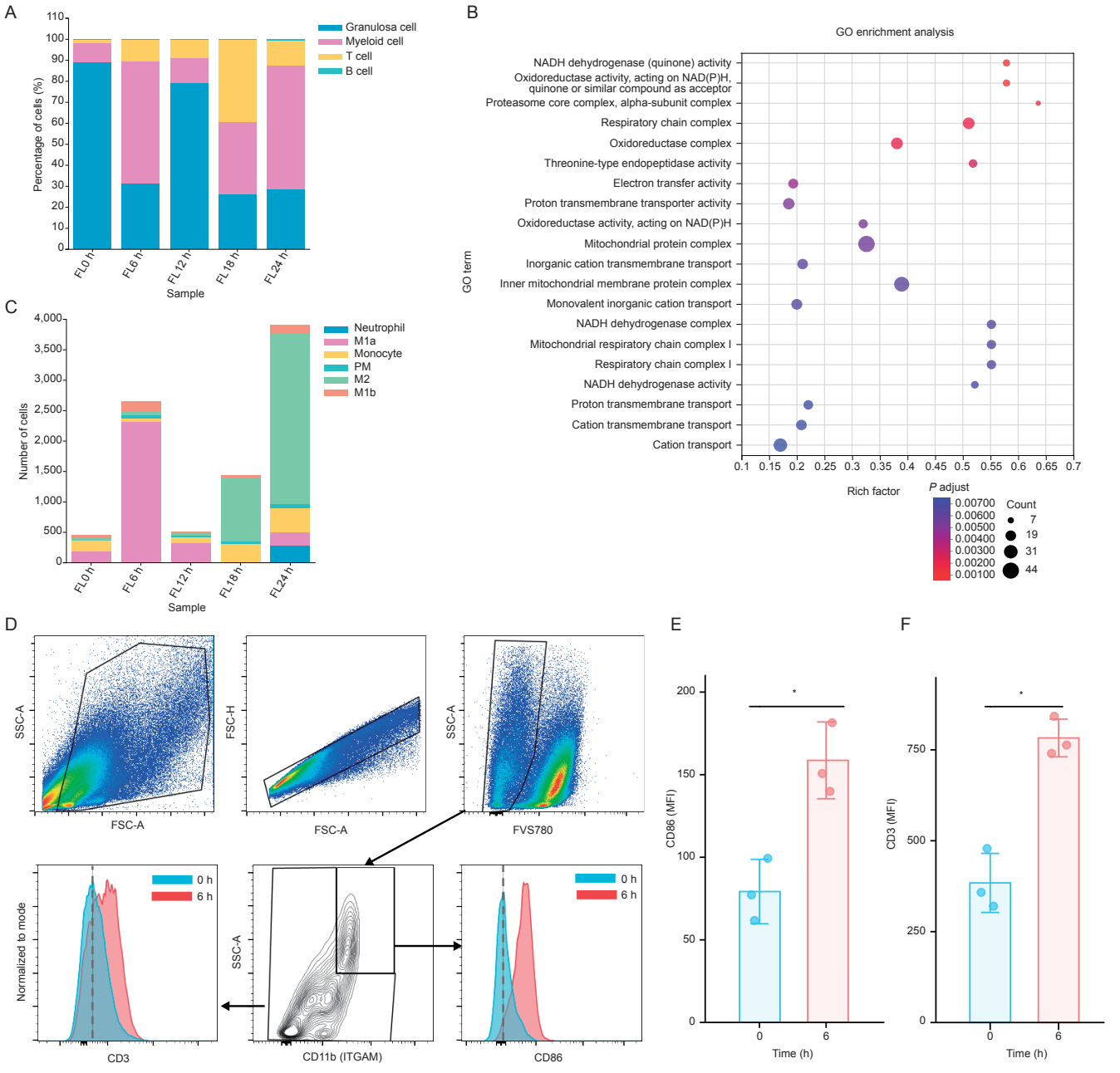

Fig. 3 Immune cells invade the follicle within 6 h after the luteinizing hormone (LH)/human chorionic gonadotropin (hCG) peak in goats. A, cell type proportions over time. B, GO enrichment terms for differential genes by comparing samples from 0 h and 6 h. C, myeloid cell subtype proportions over time. D, fluorescence-activated cell sorting of goat follicular fluid (FF) at 0 and 6 h after hCG administration. E, mean fluorescence intensity of CD86 in FF cells at 0 and 6 h. F, mean fluorescence intensity of CD3 in FF cells at 0 and 6 h. *, $P<0.05$.

expression levels of several genes, notably *ID1*, *ID3*, *APOD*, *THBS1*, etc. GO analysis unveiled significant enrichment in terms related to "negative regulation of cell population proliferation", "negative regulation of smooth muscle cell proliferation", and "negative regulation of platelet activation", suggesting suppression of these cellular activities (Fig. 4-A).

3.5. Reconstructing the temporal dynamics of GCs

During ovulation, the ovaries harbor numerous follicles in various developmental stages. Thus, we focused on the temporal dynamics of GCs to elucidate changes in fate determination during follicular development and ovulation. Initially, we employed RNA velocity analysis to reveal the differentiation states of the cells. Specifically, RNA velocity based on UMAP visualization was utilized (Fig. 5-A), with the arrow direction indicating potential cell trajectories and arrow length representing trend strength. The graph illustrated that the GC 0 appeared to represent the starting state, directing towards GC 3, GC 5, GC 6, and GC 7. GC 1 and GC 2 were other developmental branches; during the latent time, they were not the initial cluster but rather at the mid-developmental stage (Fig. 5-B). GC 3 and GC 4 appeared to represent terminal states of development. It was noteworthy that cell annotations were consistent with the RNA velocity results.

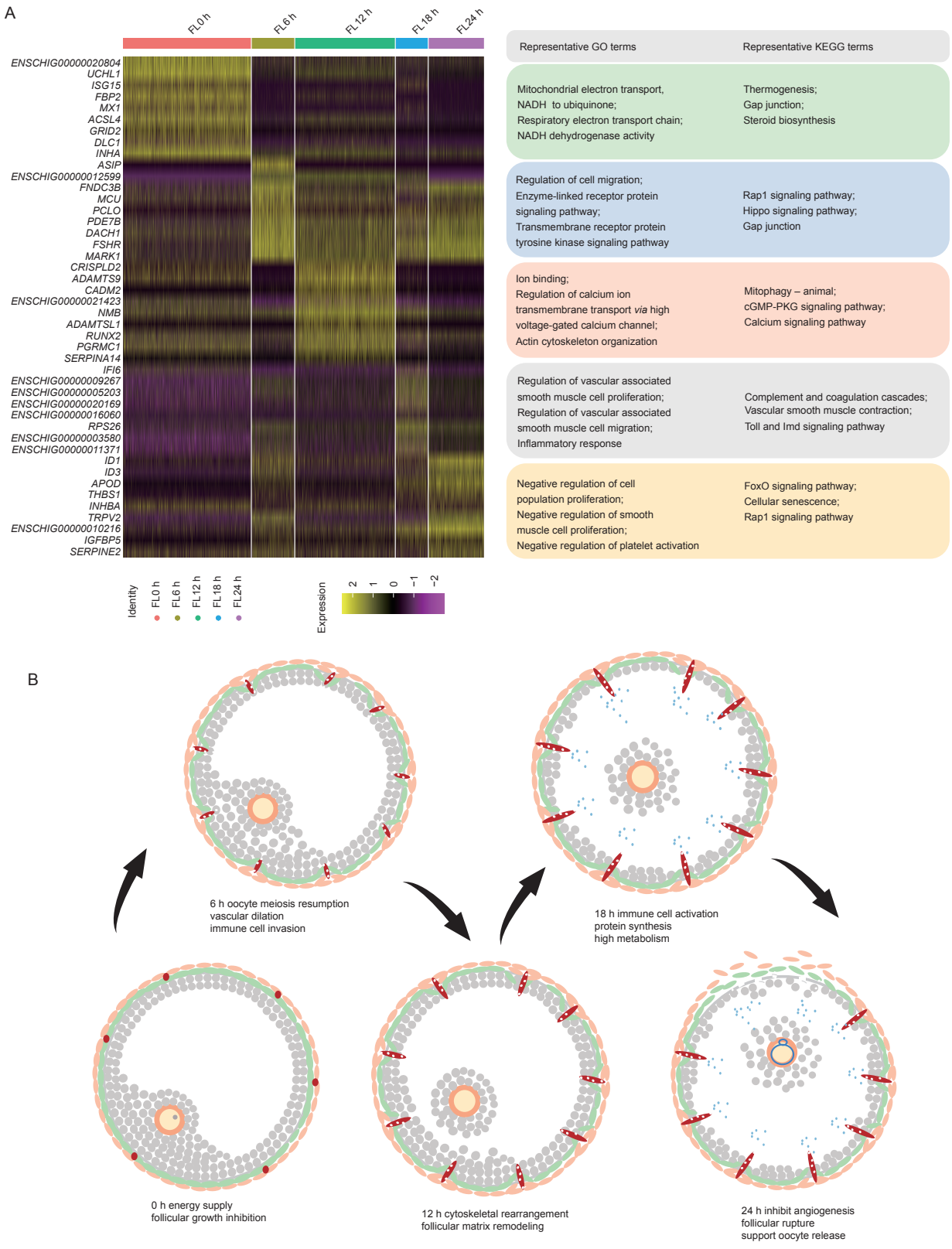

Fig. 4 Gene expression features of granulosa cells (GCs) during ovulation. A, heatmap and GO/KEGG terms of genes highly expressed at 0, 6, 12, 18, and 24 h. B, schematic diagram of follicular physiological activity at 0, 6, 12, 18, and 24 h.

After ranking the top 300 genes according to their dynamic changes along latent time, we constructed a heatmap to visualize their expression dynamics during follicular development (Fig. 5-C). At the early stage of latent time, the ribosomal gene *ENSCHIG00000025646* exhibited an initial upregulation. Subsequently, genes involved in follicle growth regulation, such as *ASPN* (Li Z *et al.* 2021); those previously associated with meiotic or reproductive processes, like *MNS1*

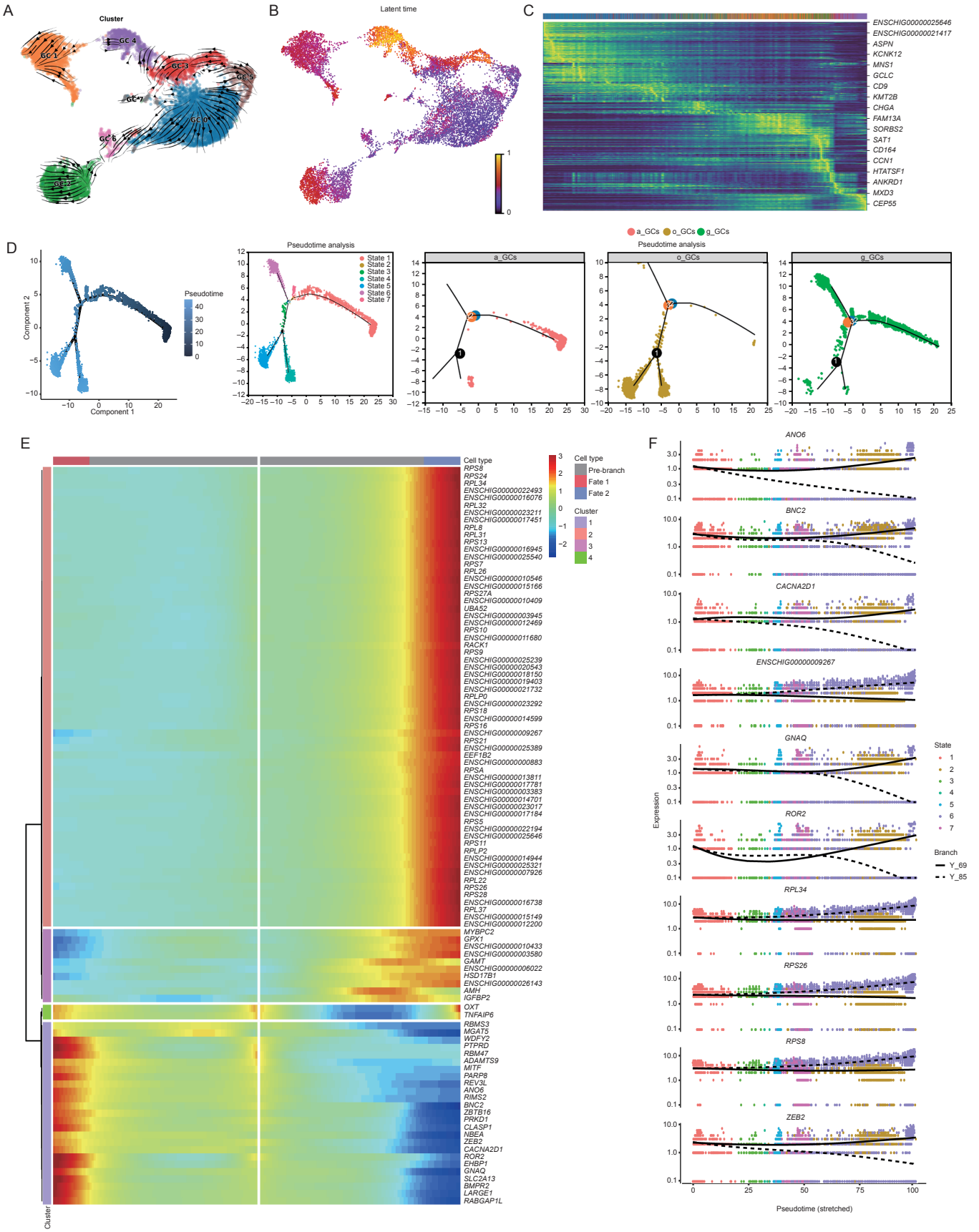

Fig. 5 Reconstructing the temporal dynamics of granulosa cells (GCs). A, results of the RNA velocity analysis of GC clusters. Arrows indicate inferred developmental directions. B, latent time in the RNA velocity analysis projected on the Uniform Manifold Approximation and Projection (UMAP) plot of the eight clusters. C, heatmap showing dynamic expression of representative genes in GCs along latent time. D, pseudotime trajectories of GCs and the distribution of GC subtypes along the pseudotime trajectories. E, heatmap of different developmental stages of GCs. F, the earliest activated or repressed top 10 genes in pseudotime.

(Hotta *et al.* 1995); regulators of oxidative stress, including *GCLC* (Liu *et al.* 2023); and genes controlling inflammatory responses, such as *CD9*, *CD164*, *CCN1* and *ANKRD1* (Huang *et al.* 2013; Emre and Imhof 2014; Liu *et al.* 2015; Brosseau *et al.* 2018), were sequentially activated. Finally, *MXD3*, which regulates cell differentiation and apoptosis (Zhang *et al*. 2021), and *CEP55*, which plays a crucial role in the final stages of cytokinesis (Sinha *et al*. 2019), were activated.

After inferring the trajectory, we delved into the temporal dynamics of GCs to further elucidate the changes in follicular development. Pseudotime analysis further revealed a branched trajectory of GCs, indicating divergent cell-state transitions during follicular development and ovulation (Fig. 5-D). The pre-branch region represented a shared transcriptional state before GC divergence, whereas the two post-branch trajectories corresponded to distinct functional programs. Fate 1 was enriched for ovulation-associated genes, including *OXT*, *TNFAIP6* and *ADAMTS9*, suggesting a transition toward ovulatory GCs and follicular remodeling. In contrast, Fate 2 showed higher expression of ribosomal genes and follicular growth-related genes, such as *AMH*, *HSD17B1* and *IGFBP2*, indicating a growing/antral follicle-associated program (Jarvensivu *et al*. 2015; Cedars 2022) (Fig. 5-E). These results suggest that GCs undergo branched transcriptional remodeling, with one trajectory associated with ovulatory transition and another associated with follicular growth or maintenance. Furthermore, we listed the top 10 genes with the most pronounced alterations in expression along the pseudotime axis, where the temporal progression is represented along the abscissa. An expedited emergence of either an ascending or descending expression trend signifies an earlier onset of activation or inhibition. Notably, *ANO6*, *BNC2*, *CACNA2D1*, *GNAQ*, and *ZEB2* displayed a significant upregulation during ovulatory follicle maturation and a concurrent downregulation during follicle growth (Fig. 5-F), suggesting that these genes were activated earliest during the development of an ovulatory follicle and may be key regulatory genes for ovulatory follicle formation.

3.6. Cellular communication during ovulation

FF harbors diverse cell types and bioactive compounds, including hormones, growth factors, proteins, peptides, amino acids, and carbohydrates. These components engage in intricate interactions mediated by cytokines, signaling pathways, and other molecular mechanisms to regulate follicular growth, development, maturation, and ovulation. To explore these interactions, we employed CellPhoneDB to analyze the crosstalk between GC subtypes and myeloid cell subtypes. As shown in Fig. 6-A, the interaction between GCs and macrophages was prominent, while minimal interaction was observed between GCs and monocytes or neutrophils. Notably, o_GCs displayed the most robust interaction with macrophages. Consequently, a ligand–receptor analysis between them was performed (Fig. 6-B), revealing several interesting findings. For instance, ligand–receptor pairs between o_GCs and macrophages were associated with angiogenesis, vascular permeability, and endothelial cell migration, due to the significant expression of *NRP1* and *CD36* in M2 and PM and high expression of *THBS1* in M1a (Hu and Jiang 2016; Bai *et al.* 2020) (Fig. 6-C). Moreover, we identified numerous ligand–receptor pairs involved in regulating cell adhesion and migration, such as *SEMA7A-PLXNC1*, *PTPRD-IL1RAP*, *LPAR3-ADGRE5*, *LPAR1-ADGRE5*, *MPZL1-MPZL1*, and *COL4A2-ADGRG6*, whose expression levels were increased in o_GCs (Yan *et al.* 2017; Andrews *et al.* 2019; Feng *et al.* 2022; Xiao *et al.* 2022). Furthermore, our findings demonstrated the regulatory role of macrophages in oocyte maturation. Specifically, M1a cells exhibit high expression of *EREG*, which plays a crucial role in promoting meiotic resumption in oocytes (Shimada *et al.* 2016). Additionally, we identified several ligand–receptor interactions associated with *APP*, such as *APP* with *CD74*, APP with *SORL1*, and *APP* with *TNFRSF21* (Matsuda *et al.* 2009; Dong *et al.* 2017).

4. Discussion

Ovulation, a complex and intricate process, relies significantly on the microenvironment of FF for the facilitation of oocyte maturation and ovulation. Our aim was to comprehensively characterize the cell populations and their functional dynamics during ovulation. Given that the typical ovulation time in goats is 24–30 h after the LH/hCG peak, we collected ovarian samples at 0, 6, 12, 18, and 24 h after hCG injection for analysis. Through transcriptomic analysis, we established the inaugural atlas of the preovulatory follicular microenvironment in goats, delineating 4 primary cell types: GCs, T cells, B cells, and myeloid cells. GCs and myeloid cells constitute the predominant cell types in FF. Therefore, we focused our research on them and subdivided GCs into 3 subtypes, g_GCs, o_GCs, and a_GCs, which deviate from the conventional GC classification. In both humans and mice, GCs are typically classified into early GCs, mural granulosa cells (mGCs), cumulus cells (CCs), and luteal GCs based on their functional roles (Fan and Chuva de Sousa Lopes 2021; Li S *et al*. 2021). Although specific studies on goats are lacking, sheep researchers have delineated similar classifications (Ge *et al.* 2023). However, our data analysis revealed no significant differences in marker gene expression between common CCs and mGCs (Appendix C-e and f). Consistent with our research findings, similar situations have been mentioned in some literature, such as in human preovulatory follicles and small antral follicles (Fan *et al.* 2021; Wu *et al.* 2022). Furthermore, we categorized myeloid cells within FF into 6 subtypes: M1a, M2, M1b, PM, monocytes, and neutrophils. This approach not only validates the presence of immune cells in preovulatory follicles but also offers a comprehensive classification of myeloid cells. We identified a proliferative macrophage population in FF, suggesting an intrafollicular proliferation rather than peripheral blood origin. However, we did not detect the presence of dendritic cells, mast cells, and natural killer cells in our data, despite reports of their involvement in ovulation in other studies. Mast cells in mouse follicles have been shown to secrete chemokines to recruit inflammatory cells and degrade the extracellular matrix to weaken follicles (Szukiewicz *et al.* 2007). Human ovarian natural killer cells secrete cytokines

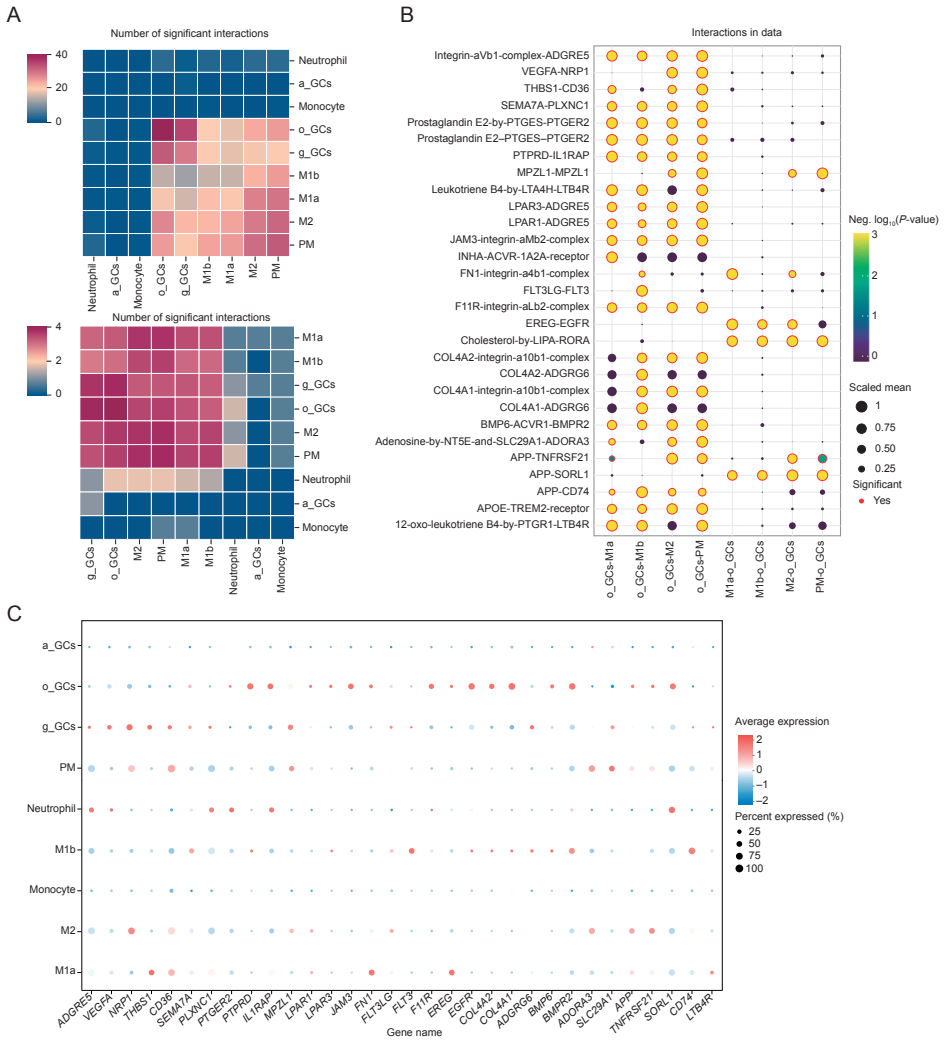

Fig. 6 Cellular communication during ovulation. A, heatmap showing interactions between different cell types. B, the interaction between ovulating granulosa cells (o_GCs) and macrophage subtypes. a_GCs, atretic granulosa cells; g_GCs, growing granulosa cells. C, expression levels of receptors or ligands in cells.

to promote inflammation, eliminate damaged cells, and stimulate angiogenesis (Yang *et al.* 2011), while dendritic cells present antigens to activate T cells (Wu *et al.* 2022). These discrepancies may be due to sampling variability or species differences. With further research, these phenomena may be elucidated.

After identifying the cell types in the FF, we analyzed their temporal characteristics during the ovulation process. Notably, we observed a significant increase in immune cell numbers in the FF at 6 h post-LH/hCG surge, consistent with previous observations in rats (Oakley *et al.* 2010). Interestingly, while oocyte maturation occurs within 12 h in rats compared to 24 h in goats, immune cell infiltration occurs at 6 h post-LH/hCG surge in both species. In humans, immune cell infiltration into ovulatory follicles differs from that in these species, occurring within 12 h post-LH/hCG surge, although human ovulation takes longer, approximately 36 h post-LH/hCG surge (Spanel-Borowski 2011). Rabbits stimulated for ovulation by mating exhibit immune cell infiltration 8 h postcoitus and 2 h before ovulation (Zachariae and Jensen 1958). This implies that immune cell infiltration may not directly correlate with ovulation duration and that no differences are observed across species. Further experimental validation is required to elucidate underlying mechanisms. Additionally, we revealed that M1a, characterized by high expression of *IL1B* and *CD44* and having stronger pro-inflammatory effects, is the predominant immune cell type in the initial phase of ovulation in goats. Conversely, during the later periovulatory phase, there is a gradual upsurge in M2 expression, indicating a subsequent phase characterized by inflammation suppression. Macrophages in preovulatory follicles demonstrate a mixed phenotype characterized by both proinflammatory and anti-inflammatory traits, implicating their role in modulating controlled inflammatory responses while minimizing ovarian tissue damage across the time course of ovulation.

Ovulation is a highly dynamic process wherein the expression of crucial genes is regulated dynamically on a time scale of minutes to hours. GCs are the primary cell type in FF. Consequently, we elucidated the gene expression and functional dynamics in GCs within 24 h after the LH/hCG peak. At 0 h, *FBP2* and *ACSL4* provide the necessary

energy for further cellular activities, while *INHA* and *DLC1* inhibit follicle growth, preparing for the ovulation phase (Kempisty *et al.* 2012; Osipova *et al.* 2023). By 6 h, *MCU* transfers calcium ions from the cytoplasm to the mitochondrial matrix, enhancing mitochondrial energy metabolism (Weiser *et al.* 2023). *PDE7B* catalyzes the degradation of cAMP in GC, significantly influencing meiotic recovery in mammalian oocytes by modulating cAMP levels (Hetman *et al.* 2000; Gupta *et al.* 2017). *FNDC3B* regulates cell migration and may be involved in immune cell infiltration (Lin *et al.* 2016). At 12 h, genes such as *CRISPLD2*, *ADAMTS9, ADAMTSL1, RUNX2* and *SERPINA14* are activated, all of which participate in ovarian stroma remodeling in preparation for follicle rupture (Yoo *et al.* 2014; Lussier *et al.* 2017; Gao *et al.* 2018; Gaikwad *et al.* 2020). By 18 h, during the active phase of ovulation, high expression of ribosomal genes like *RPS26* is typically associated with high metabolic activity and proliferation. Cells in the ovary may require significant protein synthesis, including cytokines and chemokines, to support the inflammatory response (Nathan 2002). At 24 h, *THBS1, SERPINE2*, and *APOD* are involved in immune responses and inflammation, supporting follicle structure remodeling and oocyte release (Monard 2017; Aburima *et al.* 2021; Fyfe-Desmarais *et al.* 2023). We found that genes related to angiogenesis, cell adhesion functions, and inflammation were activated later than genes related to oocyte maturation, indicating that angiogenesis, cell adhesion functions, and inflammation occur after the initiation of oocyte meiosis. A latent time-series gene heatmap also corroborated these findings. This is consistent with the results of Wu *et al.* (2022), which found that in human preovulatory follicles, inflammatory responses and cell adhesion occur earlier, while the regulation of oocyte meiotic maturation is the latest to be triggered. Both experiments reference different time dimensions from the initiation to completion of oocyte meiosis. Generally, this temporal window typically spans from approximately 12 h to several tens of hours..

Ovulation is a precisely regulated physiological process involving the interactions of various ovarian cell types. In this study, we observed extensive interactions between immune cells and GCs. Particularly, GCs may act as important signaling initiators, regulating angiogenesis, cell adhesion, and migration by binding to receptors or ligands on macrophages. Leukocyte recruitment relies on the expression of cell adhesion molecules. This illustrates the regulatory role of GCs in immune cell infiltration. It was noteworthy that M1a significantly expresses *EREG*, participating in the regulation of oocyte maturation through interaction with GCs' *EGFR*. Interestingly, Wu *et al.* (2022) also identified GCs with cell adhesion functions and macrophages expressing *EREG* in preovulatory follicles of humans, which not only corroborates our findings but also underscores the similarity and homology of mammalian reproductive systems. Additionally, we discovered numerous receptor pairs related to *APP* expression between GCs and macrophages. The binding of *APP* to *CD74* diminishes its cleavage within endosomes, thus mitigating Aβ generation. Different alleles of *APOE* influence Aβ clearance and aggregation. The interaction of *SORL1* with *APP* facilitates its trafficking from the cytoplasm to the Golgi apparatus, thereby curbing *APP* cleavage and Aβ production within endosomes (Matsuda *et al.* 2009; Dong *et al.* 2017). These ligand–receptor pairs may be involved in APP processing. The concentration of the *APP* cleavage product Aβ may be closely related to oocyte and embryo development (Duan *et al.* 2014), a possibility suggested by our ligand-receptor analysis. However, the specific pathways and mechanisms involved require further investigation.

5. Conclusion

This study established a temporal single-cell transcriptomic atlas of the ovulatory follicular microenvironment in Chuanzhong black goats. By analyzing FF at multiple time points after hCG administration, we identified the major cell populations and myeloid cell subtypes involved in ovulation and characterized the dynamic gene-expression programs of GCs during follicular maturation, ovulatory transition, and follicular remodeling before oocyte release. Notably, we observed a rapid increase in immune-cell infiltration within 6 h after the LH/hCG surge, with macrophage subsets representing the dominant immune component during the early ovulatory phase. Cell-cell communication analysis further suggested extensive crosstalk between ovulating GCs and macrophages, involving signaling pathways related to immune-cell recruitment, angiogenesis, cell adhesion, extracellular-matrix remodeling, and oocyte maturation. These findings indicate that granulosa cell–immune cell communication is a key regulatory feature of goat ovulation. Overall, this work provides a valuable single-cell resource for understanding mammalian ovulatory regulation and offers new insights for improving reproductive efficiency and supporting the genetic utilization of indigenous goat resources.

Acknowledgements

This work was supported by the Guangdong Seed Industry Revitalization Project, China (2022-XPY-00-010), the Guangdong-Guangxi Cooperative Technology Special Envoys Team Project, China (E230257), and the Modern Agricultural Industrial Technology System of Guangdong Province, China (2023KJ127). Sincere thanks to Leizhou Zhuangyuan Black Goat Co., China for cooperating with sample collection.

Declaration of competing interest

The authors declare that they have no conflict of interest.

Declaration of generative AI and AI-assisted technologies in the writing process

During the preparation of this manuscript, the authors used ChatGPT 3.5 for Chinese–English translation and to improve the clarity and readability of the language. All content generated was carefully reviewed and revised by the authors as necessary, and the authors take full responsibility for the final content of the article.

Ethical approval

All the experimental animal procedures complied with the relevant guidelines and regulations for the management

and welfare of experimental animals approved by the Ethics Committee of South China Agricultural University (license number: SYXK-2018-0123).

Appendices associated with this paper are available at https://doi.org/10.1016/j.jia.2024.09.029

References

Aburima A, Berger M, Spurgeon B E J, Webb B A, Wraith K S, Febbraio M, Poole A W, Naseem K M. 2021. Thrombospondin-1 promotes hemostasis through modulation of cAMP signaling in blood platelets. *Blood*, **137**, 678–689.

Andrews L P, Yano H, Vignali D A A. 2019. Inhibitory receptors and ligands beyond PD-1, PD-L1 and CTLA-4: Breakthroughs or backups. *Nature Immunology*, **20**, 1425–1434.

Bai J, Xia M, Xue Y, Ma F, Cui A, Sun Y, Han Y, Xu X, Zhang F, Hu Z, Liu Z, Liu Y, Cai G, Su W, Sun X, Wu H, Yan H, Chang X, Hu X, Bian H, *et al.* 2020. Thrombospondin 1 improves hepatic steatosis in diet-induced insulin-resistant mice and is associated with hepatic fat content in humans. *eBioMedicine*, **57**, 102849.

Brosseau C, Colas L, Magnan A, Brouard S. 2018. CD9 Tetraspanin: A new pathway for the regulation of inflammation? *Frontiers in Immunology*, **9**, 2316.

Carson S A, Kallen A N. 2021. Diagnosis and management of infertility: A Review. *The Journal of the American Medical Association*, **326**, 65–76.

Cedars M I. 2022. Evaluation of female fertility-AMH and ovarian reserve testing. *Journal of Clinical Endocrinology & Metabolism*, **107**, 1510–1519.

Choi Y, Jeon H, Brannstrom M, Akin J W, Curry T E, Jo M. 2023. A single-cell gene expression atlas of human follicular aspirates: Identification of leukocyte subpopulations and their paracrine factors. *FASEB Journal*, **37**, 22843.

Danaher P, Hasle N, Nguyen E D, Hayward K, Rosenwasser N, Alpers C E, Reed R C, Okamura D M, Baxter S K, Jackson S W. 2023. Single cell spatial transcriptomic profiling of childhood-onset lupus nephritis reveals complex interactions between kidney stroma and infiltrating immune cells. *bioRxiv*, **13**, 566503.

Direito A, Bailly S, Mariani A, Ecochard R. 2013. Relationships between the luteinizing hormone surge and other characteristics of the menstrual cycle in normally ovulating women. *Fertility and Sterility*, **99**, 279–285.

Dong H K, Gim J A, Yeo S H, Kim H S. 2017. Integrated late onset Alzheimer's disease (LOAD) susceptibility genes: Cholesterol metabolism and trafficking perspectives. *Gene*, **597**, 10–16.

Duan F H, Chen S L, Chen X, Niu J, Li P, Liu Y D, Xu L J. 2014. Follicular fluid Abeta40 concentrations may be associated with ongoing pregnancy following *in vitro* fertilization. *Journal of Assisted Reproduction and Genetics*, **31**, 1611–1620.

Duffy D M, Ko C, Jo M, Brannstrom M, Curry T E. 2019. Ovulation: Parallels with inflammatory processes. *Endocrine Reviews*, **40**, 369–416.

Dura B, Choi J Y, Zhang K, Damsky W, Thakral D, Bosenberg M, Craft J, Fan R. 2019. scFTD-seq: Freeze-thaw lysis based, portable approach toward highly distributed single-cell 3' mRNA profiling. *Nucleic Acids Research*, **47**, e16.

Emre Y, Imhof B A. 2014. Matricellular protein CCN1/CYR61: A new player in inflammation and leukocyte trafficking. *Seminars in Immunopathology*, **36**, 253–259.

Fan X, Chuva de Sousa Lopes S M. 2021. Molecular makeup of the human adult ovary. *Current Opinion in Endocrine and Metabolic Research*, **18**, 187–193.

Fan X, Moustakas I, Bialecka M, Del Valle J S, Overeem A W, Louwe L A, Pilgram G S K, van der Westerlaken L A J, Mei H, Chuva de Sousa Lopes S M. 2021. Single-cell transcriptomics analysis of human small antral follicles. *International Journal of Molecular Sciences*, **22**, 11955.

Feng J, Ouyang H, Wang J, Pan D, Sheng L, Xu C, Lin W, Hu D, Chang C, Jia D. 2022. MPZL1 upregulation promotes tumor metastasis and correlates with unfavorable prognosis in non-small cell lung cancer. *Carcinogenesis*, **43**, 919–929.

Fyfe-Desmarais G, Desmarais F, Rassart E, Mounier C. 2023. Apolipoprotein D in oxidative stress and inflammation. *Antioxidants* (Basel), **12**, 1027.

Gaikwad A S, Hu J, Chapple D G, O'Bryan M K. 2020. The functions of CAP superfamily proteins in mammalian fertility and disease. *Human Reproduction Update*, **26**, 689–723.

Gao K, Wang P, Peng J, Xue J, Chen K, Song Y, Wang J, Li G, An X, Cao B. 2018. Regulation and function of runt-related transcription factors (RUNX1 and RUNX2) in goat granulosa cells. *The Journal of Steroid Biochemistry and Molecular Biology*, **181**, 98–108.

Gao L, Zhang C, Zheng Y, Wu D, Chen X, Lan H, Zheng X, Wu H, Li S. 2023. Glycine regulates lipid peroxidation promoting porcine oocyte maturation and early embryonic development. *Journal of Animal Science*, **101**, skac425.

Ge T, Wen Y, Li B, Huang X, Jiang S, Zhang E. 2023. Single-cell sequencing reveals the reproductive variations between primiparous and multiparous Hu ewes. *Journal of Animal Science and Biotechnology*, **14**, 144.

Grondahl M L, Andersen C Y, Bogstad J, Borgbo T, Boujida V H, Borup R. 2012. Specific genes are selectively expressed between cumulus and granulosa cells from individual human pre-ovulatory follicles. *Molecular Human Reproduction*, **18**, 572–584.

Gupta A, Tiwari M, Prasad S, Chaube S K. 2017. Role of cyclic nucleotide phosphodiesterases during meiotic resumption from diplotene arrest in mammalian oocytes. *Journal of Cellular Biochemistry*, **118**, 446–452.

Hao Y, Hao S, Andersen-Nissen E, Mauck W M III, Zheng S, Butler A, Lee M J, Wilk A J, Darby C, Zager M, Hoffman P, Stoeckius M, Papalexi E, Mimitou E P, Jain J, Srivastava A, Stuart T, Fleming L M, Yeung B, Rogers A J, *et al.* 2021. Integrated analysis of multimodal single-cell data. *Cell*, **184**, 3573–3587.

He D, Wang D, Lu P, Yang N, Xue Z, Zhu X, Zhang P, Fan G. 2021. Single-cell RNA sequencing reveals heterogeneous tumor and immune cell populations in early-stage lung adenocarcinomas harboring EGFR mutations. *Oncogene*, **40**, 355–368.

Hetman J M, Soderling S H, Glavas N A, Beavo J A. 2000. Cloning and characterization of PDE7B, a cAMP-specific phosphodiesterase. *Proceedings of the National Academy of Sciences of the United States of America*, **97**, 472–476.

Hotta Y, Furukawa K, Tabata S. 1995. Meiosis specific transcription and functional proteins. *Annual Review of Biophysics*, **31**, 101–115.

Hu C, Jiang X. 2016. Role of NRP-1 in VEGF-VEGFR2-independent tumorigenesis. *Target Oncology*, **11**, 501–505.

Huang A F, Chen M W, Huang S M, Kao C L, Lai H C, Chan J Y. 2013. CD164 regulates the tumorigenesis of ovarian surface epithelial cells through the SDF-1α/CXCR4 axis. *Molecular Cancer*, **12**, 115.

Huang Y F, Chen L P, Zhao Y J, Zhang H, Na R S, Zhao Z Q, Zhang J H, Jiang C D, Ma Y H, Sun Y W, E G X. 2016. Complete mitochondrial genome of Chuanzhong black goat in southwest of China (*Capra hircus*). *Mitochondrial DNA Part A* (DNA Mapping, Sequencing, and Analysis), **27**, 3063–3064.

Ingram S, Mengozzi M, Sacre S, Mullen L, Ghezzi P. 2019. Differential induction of nuclear factor-like 2 signature genes with toll-like receptor stimulation. *Free Radical Biology and Medicine*, **135**, 245–250.

Jarvensivu P, Saloniemi-Heinonen T, Awosanya M, Koskimies P, Saarinen N, Poutanen M. 2015. HSD17B1 expression enhances estrogen signaling stimulated by the low active estrone, evidenced by an estrogen responsive element-driven reporter gene *in vivo*. *Chemico-Biological Interactions*, **234**, 126–134.

Kempisty B, Jackowska M, Wozna M, Antosik P, Piotrowska H, Zawierucha P, Bukowska D, Jaskowski J M, Nowicki M, Brussow K P. 2012. Expression and cellular distribution of INHA and INHB before and after *in vitro* cultivation of porcine oocytes isolated from follicles of different size. *Journal of Biomedicine and Biotechnology*, **2012**, 742829.

Li S, Chen L N, Zhu H J, Feng X, Xie F Y, Luo S M, Ou X H, Ma J Y. 2021. Single-cell RNA sequencing analysis of mouse follicular somatic cells. *Biology of Reproduction*, **105**, 1234–1245.

Li Z, Wang J, Zhao Y, Ma D, Zhao M, Li N, Men Y, Zhang Y, Chu H, Lei C, Shen W, El-Mahdy Othman O, Min L. 2021. scRNA-seq of ovarian follicle granulosa cells from different fertility goats reveals distinct expression patterns. *Reproduction in Domestic Animals*, **56**, 801–811.

Liang Y, Xing X, Beamer M A, Swindell W R, Sarkar M K, Roberts L W, Voorhees J J, Kahlenberg J M, Harms P W, Johnston A, Gudjonsson J E. 2017. Six-transmembrane epithelial antigens of the prostate comprise a novel inflammatory nexus in patients with pustular skin disorders. *Journal of Allergy and Clinical Immunology*, **139**, 1217–1227.

Lin C H, Lin Y W, Chen Y C, Liao C C, Jou Y S, Hsu M T, Chen C F. 2016. FNDC3B promotes cell migration and tumor metastasis in hepatocellular carcinoma. *Oncotarget*, **7**, 49498–49508.

Liu J, Aronow B J, Witte D P, Pope W F, La Barbera A R. 1998. Cyclic and maturation-dependent regulation of follicle-stimulating hormone receptor and luteinizing hormone receptor messenger ribonucleic acid expression in the porcine ovary. *Biology of Reproduction*, **58**, 648–658.

Liu N, Si X, Ji Y, Yang Q, Bai J, He Y, Jia H, Song Z, Chen J, Yang L, Zeng S, Yang Y, Wu Z. 2023. l-Proline improves the cytoplasmic maturation of mouse oocyte by regulating glutathione-related redox homeostasis. *Theriogenology*, **195**, 159–167.

Liu X H, Bauman W A, Cardozo C. 2015. ANKRD1 modulates inflammatory responses in C2C12 myoblasts through feedback inhibition of NF-kappaB signaling activity. *Biochemical and Biophysical Research Communications*, **464**, 208–213.

Lussier J G, Diouf M N, Levesque V, Sirois J, Ndiaye K. 2017. Gene expression profiling of upregulated mRNAs in granulosa cells of bovine ovulatory follicles following stimulation with hCG. *Reproductive Biology and Endocrinology*, **15**, 88.

Mantri M, Zhang H H, Spanos E, Ren Y A, De Vlaminck I. 2024. A spatiotemporal molecular atlas of the ovulating mouse ovary. *Proceedings of the National Academy of Sciences of the United States of America*, **121**, e2317418121.

Matsuda S, Matsuda Y, D'Adamio L. 2009. CD74 interacts with APP and suppresses the production of Abeta. *Molecular Neurodegeneration*, **4**, 41.

Monard D. 2017. SERPINE2/Protease Nexin-1 *in vivo* multiple functions: Does the puzzle make sense? *Seminars in Cell & Developmental Biology*, **62**, 160–169.

Mrdjen D, Pavlovic A, Hartmann F J, Schreiner B, Utz S G, Leung B P, Lelios I, Heppner F L, Kipnis J, Merkler D, Greter M, Becher B. 2018. High-dimensional single-cell mapping of central nervous system immune cells reveals distinct myeloid subsets in health, aging, and disease. *Immunity*, **48**, 599.

Nathan C. 2002. Points of control in inflammation. *Nature*, **420**, 846–852.

Oakley O R, Kim H, El-Amouri I, Lin P C, Cho J, Bani-Ahmad M, Ko C. 2010. Periovulatory leukocyte infiltration in the rat ovary. *Endocrinology*, **151**, 4551–4559.

Osipova E, Barsacchi R, Brown T, Sadanandan K, Gaede A H, Monte A, Jarrells J, Moebius C, Pippel M, Altshuler D L, Winkler S, Bickle M, Baldwin M W, Hiller M. 2023. Loss of a gluconeogenic muscle enzyme contributed to adaptive metabolic traits in hummingbirds. *Science*, **379**, 185–190.

Owen C M, Jaffe L A. 2023. Luteinizing hormone stimulates ingression of mural granulosa cells within the mouse preovulatory follicle. *Biology of Reproduction*, **110**, 288–299.

Rahman N A, Rao C V. 2009. Recent progress in luteinizing hormone/human chorionic gonadotrophin hormone research. *Molecular Human Reproduction*, **15**, 703–711.

Ruvolo P P, Ma H, Ruvolo V R, Zhang X, Post S M, Andreeff M. 2020. LGALS1 acts as a pro-survival molecule in AML. *Biochimica et Biophysica Acta-Molecular Cell Research*, **1867**, 118785.

Sayasith K, Bouchard N, Dore M, Sirois J. 2008. Regulation of bovine tumor necrosis factor-α-induced protein 6 in ovarian follicles during the ovulatory process and promoter activation in granulosa cells. *Endocrinology*, **149**, 6213–6225.

Shimada M, Umehara T, Hoshino Y. 2016. Roles of epidermal growth factor (EGF)-like factor in the ovulation process. *Reproductive Medicine and Biology*, **15**, 201–216.

Sinha D, Duijf P H G, Khanna K K. 2019. Mitotic slippage: An old tale with a new twist. *Cell Cycle*, **18**, 7–15.

Solier S, Muller S, Caneque T, Versini A, Mansart A, Sindikubwabo F, Baron L, Emam L, Gestraud P, Pantos G D, Gandon V, Gaillet C, Wu T D, Dingli F, Loew D, Baulande S, Durand S, Sencio V, Robil C, Trottein F, *et al.* 2023. A druggable copper-signalling pathway that drives inflammation. *Nature*, **617**, 386–394.

Spanel-Borowski K. 2011. Ovulation as danger signaling event of innate immunity. *Molecular and Cellular Endocrinology*, **333**, 1–7.

Szukiewicz D, Pyzlak M, Klimkiewicz J, Szewczyk G, Maslinska D. 2007. Mast cell-derived interleukin-8 may be involved in the ovarian mechanisms of follicle growth and ovulation. *Inflammation Research*, **56**, S35–S36.

Trapnell C, Cacchiarelli D, Grimsby J, Pokharel P, Li S, Morse M, Lennon N J, Livak K J, Mikkelsen T S, Rinn J L. 2014. The dynamics and regulators of cell fate decisions are revealed by pseudotemporal ordering of single cells. *Nature Biotechnology*, **32**, 381–386.

Turathum B, Gao E M, Chian R C. 2021. The function of cumulus cells in oocyte growth and maturation and in subsequent ovulation and fertilization. *Cells*, **10**, 2292.

Wang Q, Tang S B, Song X B, Deng T F, Zhang T T, Yin S, Luo S M, Shen W, Zhang C L, Ge Z J. 2018. High-glucose concentrations change DNA methylation levels in human IVM oocytes. *Molecular Human Reproduction*, **33**, 474–481.

Weiser A, Hermant A, Bermont F, Sizzano F, Karaz S, Alvarez-Illera P, Santo-Domingo J, Sorrentino V, Feige J N, De Marchi U. 2023. The mitochondrial calcium uniporter (MCU) activates mitochondrial respiration and enhances mobility by regulating mitochondrial redox state. *Redox Biology*, **64**, 102759.

Wu H, Zhu R, Zheng B, Liao G, Wang F, Ding J, Li H, Li M. 2022. Single-cell sequencing reveals an intrinsic heterogeneity of the preovulatory follicular microenvironment. *Biomolecules*, **12**, 231.

Xiao P, Guo S, Wen X, He Q T, Lin H, Huang S M, Gou L, Zhang C, Yang Z, Zhong Y N, Yang C C, Li Y, Gong Z, Tao X N, Yang Z S, Lu Y, Li S L, He J Y, Wang C, Zhang L, *et al.* 2022. Tethered peptide activation mechanism of the adhesion GPCRs ADGRG2 and ADGRG4. *Nature*, **604**, 771–778.

Yan H, Wu L, Shih C, Hou S, Shi J, Mao T, Chen W, Melvin B, Rigby R J, Chen Y, Jiang H, Friedel R H, Vinuesa C G, Qi H. 2017. Plexin B2 and semaphorin 4C guide T cell recruitment and function in the germinal center. *Cell Reports*, **19**, 995–1007.

Yang Z, Kong B, Mosser D M, Zhang X. 2011. TLRs, macrophages, and NK cells: Our understandings of their functions in uterus and ovary. *International Immunopharmacology*, **11**, 1442–1450.

Yoo J Y, Shin H, Kim T H, Choi W S, Ferguson S D, Fazleabas A T, Young S L, Lessey B A, Ha U H, Jeong J W. 2014. CRISPLD2 is a target of progesterone receptor and its expression is decreased in women with endometriosis. *PLoS ONE*, **9**, e100481.

Zachariae F, Jensen C E. 1958. Studies on the mechanism of ovulation: Histochemical and physico-chemical investigations on genuine follicular fluids. *Acta Endocrinologica* (Copenhagen), **27**, 343–355.

Zaniker E J, Babayev E, Duncan F E. 2023. Common mechanisms of physiological and pathological rupture events in biology: Novel insights into mammalian ovulation and beyond. *Biological Reviews of the Cambridge Philosophical Society*, **98**, 1648–1667.

Zhang X, He X, Li Y, Xu Y, Chen W, Liu X, Hu X, Xiong L, Xu X. 2021. MXD3 as an immunological and prognostic factor from pancancer analysis. *Frontiers in Molecular Biosciences*, **8**, 702206.